Polarization of molecular targets using infrared stimulated Raman adiabatic passage

Nandini Mukherjee and Richard N. Zare[a)]
Department of Chemistry, Stanford University, Stanford, California 94305-5080, USA

(Received 24 May 2010; accepted 15 July 2010; published online 2 September 2010)

We suggest that infrared stimulated Raman adiabatic passage, a coherent multiple excitation process, can be used to create a superposition of $(2J+1)$ highly correlated M-state sublevels of a rigid rotor molecule with vibrational level v and rotational level J. This method employs the $(v=0,J-2)$ to $(v=2,J)$ S-branch transition, which is carried out in a counterintuitive manner in which the $v=1$ to $v=2$ transition is pumped prior to the $v=0$ to $v=1$ transition, causing nearly complete population transfer to the $v=2$ final level. We use perpendicular and parallel linearly polarized infrared excitation (biaxial excitation). Specifically, the perpendicular polarization connects the $v=1$ intermediate level to the final vibrational level $v=2$, and the parallel polarization connects the initial level $v=0$ to the intermediate level $v=1$. By this means we break the cylindrical symmetry for an ensemble of vibrationally excited molecules in a rovibrational eigenstate $(v=2,J)$. The angular momentum polarization is determined by the relative phases rather than by the populations of the magnetic M-sublevels. For the phase correlated ensemble, the angular momentum polarization can be considered as a purely quantum mechanical effect. Using a fully general density matrix treatment, we illustrate this approach by considering a beam of carbon monoxide (CO) molecules. We find that significant polarization for $J=2$, 5, and 10 can be achieved with a cw infrared laser source having modest power ($\sim$100 mW/mm^2). We believe that this technique is a general one and may offer an experimentally accessible new platform for different applications, from scattering studies with M-state entangled ensembles of molecules to logic gate operations of a quantum computer. © *2010 American Institute of Physics*. [doi:10.1063/1.3475523]

I. INTRODUCTION

To prepare polarized molecular targets, various linear and nonlinear optical excitation methods have been developed. These include optical pumping via electronic transitions[1] and the dipole-allowed infrared transitions to cause population transfer from $(v=0,J'')$ to $(v'=1,J')$.[2–4] Although optical pumping may significantly polarize the ground state, it cannot generate polarization in the excited vibrational levels that is often desirable in collision studies. Infrared pumping creates polarization only in the limit of weak excitation (low population transfer). It is also possible to prepare polarized targets in the excited vibrational level v' by stimulated Raman pumping[5] using high-power visible or UV lasers, but again this technique suffers from incomplete population transfer. Another approach is chirped adiabatic Raman passage,[6] which uses the selection rule dependence of the excitation rate on M to create the molecular polarization in the excited level, but this nonlinear optical method demands high power and control on the temporal and spectral shapes of the laser pulses. We should note that in all these methods each M-sublevel acts independently, implying that there are no phase relationships among them. In this case, an optically polarized molecular ensemble follows the classical distribution, determined by the M-state population.[7]

We present a different approach involving the preparation of coherently coupled magnetic sublevels in which we control both the population and the relative phase of the interfering M-sublevels. The coherent superposition state is prepared using multiple infrared excitations in a counterintuitive manner via infrared stimulated Raman adiabatic passage (IR STIRAP).[8–12] Using this procedure, nearly complete population transfer to $v=2,J$ level is achieved and a time-independent superposition state is formed for the spatial confinement of the angular momentum vector $\boldsymbol{J}$. The orientational distribution of $\boldsymbol{J}$ is no longer described only by the relative populations of the M-sublevels. The $\boldsymbol{J}$-distribution has a purely quantum mechanical character determined by the relative phases of the M-sublevels. Using resonant excitation with elliptically polarized light, Milner *et al.*[13,14] have created a similar nonclassical $\boldsymbol{J}$-distribution in a vibrational ground state. Their preparation of the angular momentum state relies on optically pumping a fraction $(\approx 1/J)$ of the population into a dark state, formed by coherently mixing the magnetic sublevels of the atomic or molecular ground state. The timescale of trapping is determined by the spontaneous emission rate of a lifetime broadened upper rovibrational level. On the contrary, IR STIRAP does not use optical pumping to create a nonclassical $\boldsymbol{J}$-distribution in a two-photon excited vibrational level. A dark state or a trapped state is prepared from the superposition of the ground and the two-photon excited rovibrational levels. This superposition state is then adiabatically changed using the counterintuitive sequence of optical pulses, aligning it with the target

a)Electronic mail: zare@stanford.edu.

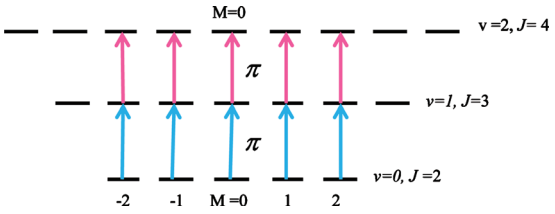

FIG. 1. S(2) transition with two resonant π-polarized photons.

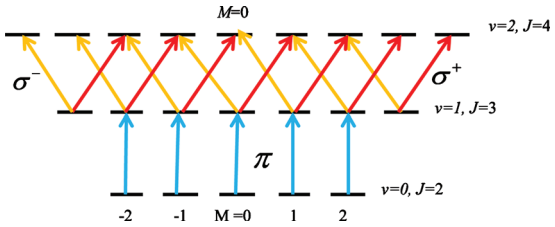

FIG. 2. S(2) transition with biaxial excitation, i.e., combined π- and σ-polarized photons. The blue arrows represent π-polarized photons and red and yellow arrows represent σ^+- and σ^--polarized photons, respectively.

state at the end of excitation, thus achieving nearly complete population transfer.[8–12] In this paper, we demonstrate how IR STIRAP can be used to create a polarized target by coherently tying together the magnetic M-sublevels of a two-photon excited rovibrational eigenstate within the ground electronic surface.

To appreciate fully the implication of phase correlation, also called the Zeeman coherence, let us consider the case of an S-branch two-photon rovibrational transition $(v=0,J-2) \rightarrow (v=2,J)$, denoted by S(J−2), with two resonant π-polarized photons. Figure 1 shows the case for $J=2$ as the initial state. When both the $v=0 \rightarrow v=1$ and $v=1 \rightarrow v=2$ transitions of the vibrational ladder are excited using π-polarized parallel light, different M-sublevels are decoupled because of the $\Delta M=0$ selection rule. As a result, there are no definite phase relationships among the excitation amplitudes of the individual M-sublevels of the $(v=2,J)$ rovibrational level. In the absence of any phase relationship between the Zeeman substates, the $\boldsymbol{J}$-polarization is described by a cylindrically symmetric distribution defined by the nonzero alignment parameter[15,16]

$$A_0^{(2)} = \left\langle \frac{3M^2 - J(J+1)}{J(J+1)} \right\rangle = \sum_{M=-J}^{J} |C_M|^2 \frac{3M^2 - J(J+1)}{J(J+1)}. \tag{1}$$

It can be inferred from Eq. (1) that in case of saturation or in the case of complete population transfer using STIRAP with two resonant π-polarized photons, the uniform population distribution in the excited rovibrational (v,J,M) levels substantially reduces the molecular alignment. For example, when $|C_M|^2$ becomes independent of M in the case of complete saturation with a large rotational quantum number J, $A_0^{(2)} \rightarrow 0$. The situation corresponds to a spherically symmetric distribution of the rigid rotor axis defined per solid angle element, which is given by

$$f(\theta,\varphi) \rightarrow \sum_{M=-J}^{J} |Y_{JM}(\theta,\phi)|^2 = 1. \tag{2}$$

How is molecular alignment altered in presence of Zeeman coherence? To answer this question we consider the case of an S$(J-2)$ transition using combined π- and σ-polarized light as shown in Fig. 2 for $J=2$. Here a phase correlation is established between all the magnetic M-sublevels both in the upper as well as in the intermediate rovibrational levels by the Raman-type coupling of the σ^+ (red) and σ^- (yellow) circularly polarized photons. The phase entangled circularly polarized field components may be derived from an orthogonal linearly polarized (biaxial) or from an elliptically polarized light source. In this case, the amplitude C_M of the Zeeman sublevel M in the two-photon excited level $(v=2,J)$ includes the interference of two channels involving the π and a σ^+ or a σ^- photon. The combination of parallel and perpendicular excitation creates an entangled state for the two-photon-excited molecular ensemble by coherently tying together the M-sublevels of the $(v=2,J)$ rovibrational level. For such an ensemble, the cylindrical symmetry is broken, creating a higher spatial order for the angular momentum $\boldsymbol{J}$-polarization described by a set of alignment parameters $A_0^{(2)}(J)$ and $A_{\pm 2}^{(2)}(J)$ (Refs. 15 and 16)

$$A_{\pm 2}^{(2)}(J) \propto \frac{1}{J(J+1)} \sum_{M=-J}^{J} \rho^J_{(M)(M\pm 2)} [J(J+1) - M(M \pm 1)]^{1/2} \times [J(J+1) - (M \pm 1)(M \pm 2)]^{1/2}, \tag{3}$$

where $\rho^J_{(M)(M\pm 2)}$ represents the coherence between the magnetic sublevels M and $M \pm 2$ of the final rovibrational level. Equivalently, we might describe the spatial distribution of the rigid rotor axes defined per solid angle element by

$$f(\theta,\phi) = \sum_{M=-J}^{J} |C_M|^2 |Y_{JM}(\theta,\phi)|^2 + \sum_{M \neq N} \overline{C_N^* C_M} Y_{JM}(\theta,\phi) Y_{JN}^*(\theta,\phi). \tag{4}$$

$\overline{C_M C_N^*}$ is the ensemble averaged correlation of the Zeeman amplitudes and defines the density matrix element ρ^J_{MN}. Note that in the absence of Zeeman coherence, the ensemble averaged terms $\overline{C_M C_N^*}=0$ for $M \neq N$. From Eqs. (3) and (4), it can be seen intuitively that even in the presence of complete saturation or complete population transfer approaching a uniform Zeeman distribution ($|C_M|^2$ being independent of M), there can be substantial polarization for the angular momentum $\boldsymbol{J}$ and a corresponding strong anisotropy in the rigid rotor axes distribution. The molecular polarization arises from the interference term, the second term on the right hand side of Eq. (4), which is proportional to the nonzero value of the off-diagonal density matrix elements $\rho^J_{MN}=\overline{C_M C_N^*}$.

The entanglement of M-sublevels, however, substantially complicates the IR STIRAP dynamics. In general, for the S$(J-2)$ transition there are $6J-3$ quantum levels involved in the dynamics of IR STIRAP. For the successful STIRAP operation, a zero (or more technically a near zero) eigenvalue adiabatic eigenstate[10] of the $(6J-3)\times(6J-3)$ Hamiltonian must be formed from the superposition of the M-sublevels of the ground and excited states for a given

choice of the optical polarization. Under excitation by a delayed sequence of infrared pulses applied in a counterintuitive fashion, such an eigenstate will adiabatically carry the entire (or more technically almost the entire) ground-state population to the final excited state. It is important to realize that in the presence of degenerate magnetic sublevels, the evolution of the adiabatic eigenstates becomes sufficiently complex to limit the population transfer as expected in an ideal STIRAP for a nondegenerate three-level system. In the presence of degenerate eigenstates, even using counterintuitive sequence of Stokes and pump pulses, it is impossible to prepare the system in a single adiabatic eigenstate that perfectly matches with the ground state at the beginning of the interaction and connects to the target state at the end of the interaction. Moreover, in the absence of a single ground state, the initial alignment of the zero eigenvalue adiabatic eigenstate with the ground magnetic sublevels (incoherent superposition) will not be perfect. Previously, Bergmann and co-workers[17] considered the relatively simpler case of an S(0) transition in the rotating wave approximation (RWA) using the Schrödinger representation. This is the situation of a nondegenerate ground state which can be perfectly aligned with the adiabatic eigenstate to allow complete population transfer to the two-photon target state. We have used a density matrix analysis to describe the S(0) STIRAP with combined parallel and perpendicular transition.[8] With increasing values of J, in the presence of the interference of excitation channels, it becomes difficult, if not impossible, to inspect or to analytically determine the amplitudes and phases of all the $2J+1$ magnetic sublevels. Using a graphical technique,[18] we develop a comprehensive density matrix treatment to describe the multidimensional STIRAP for an arbitrary rotational quantum number J. The density matrix approach has the advantage of describing the dephasing phenomena arising either from the finite interaction time, or the finite laser bandwidth, or both. A numerical analysis is used to determine the desired adiabatic eigenstate, the Zeeman coherence, the population transfer, and the angular momentum polarization.

The theory is applied to isolated carbon monoxide (CO) molecules in a molecular beam using the delayed infrared pulse excitation in a counterintuitive sense. We find that using a modest laser powers significant (>90%) population transfer and alignment is possible in the presence of a strong phase entanglement for $J=2,5,10$. For high-J states, the population transfer is limited owing to the quantum interference but is still quite large.

II. DENSITY MATRIX TREATMENT

We denote the initial level by $(v=0,J'')$, the intermediate level by $(v=1,J')$, and the final level by $(v=2,J)$. We consider an S(J'') transition using a $\hat{z}$ and a $\hat{x}$ linearly polarized light resonantly tuned to the π and σ transitions. The $\hat{z}$- and $\hat{x}$-polarized optical fields can be expressed as follows:

$$\vec{E}_P(\omega_P) = \hat{z}E_P e^{i\omega_P t} + c\,.\,c\,.\,, \tag{5a}$$

$$\vec{E}_S(\omega_S) = \hat{x}E_S e^{i\omega_S t} + cc = \frac{1}{\sqrt{2}}(\hat{\sigma}_- - \hat{\sigma}_+)E_S e^{i\omega_S t} + cc, \tag{5b}$$

where $\hat{\sigma}_-$ and $\hat{\sigma}_+$ are the spherical unit vectors representing the right E_- and left E_+ circularly polarized optical fields. The optical frequencies ω_P and ω_S are resonantly tuned to the $(v=0,J'')\rightarrow(v=1,J')$ and $(v=1,J')\rightarrow(v=2,J)$ transitions, respectively. The degenerate three-level rovibrational system is described by a multidimensional density matrix $\hat{\rho}$, whose diagonal elements are expressed by $\rho_M^J \equiv \rho_{(JM)(JM)}$, representing the population of the magnetic sublevel M of a rovibrational level (v,J), where $J \equiv J''$, J', or J. The off-diagonal density matrix elements of $\hat{\rho}$ are used to represent the phase correlation of the various quantum states coupled by the nonlinear optical interactions of π- and σ-polarized light. For example, $\rho_{(JM)(J'M')}$ represents the ensemble averaged phase correlation for the superposition of the quantum states (JM) and (J',M'). Because we are only interested in the Fourier components of the density matrix elements that are resonantly excited by the optical interactions, we expand $\rho_{(JM)(J'M')}$ in the following way:[18]

$$\rho_{(JM)(J'M')} = \sigma_{(JM)(J'M')}(\omega)e^{i\omega t} + \sigma_{(JM)(J'M')}(-\omega)e^{-i\omega t}, \tag{6}$$

where $\sigma_{(JM)(J'M')}(\omega)$ is the slowly varying Fourier amplitude of the optically driven coherence at frequency ω. The density matrix amplitude $\sigma_{(JM)(J'M')}(\omega)$, representing the coherent superposition of the quantum states (JM) and (J',M') at frequency ω, is created by the sum and difference frequency mixing of the interacting optical fields. For example, the Zeeman coherence $\sigma^J_{(M)(M')}$ at $\omega=0$, representing the coherent coupling of the M-sublevels in a given J state, is created by the difference frequency mixing of the circularly polarized optical fields $\hat{\sigma}_-$ and $\hat{\sigma}_+$ at frequency ω_S

In presence of the optical fields, the equations for the slowly varying Fourier components of the density matrix are derived using a diagrammatic technique.[18] Figures 3 and 4 show the typical interaction diagrams that are used to derive equations for the slowly varying density matrix elements involved in the $v=0\rightarrow v=2$ transitions. Figure 3 presents the interference of excitation pathways in an N-type interaction, affecting the density matrix component $\sigma_{(J'M)(JM+1)}$ between the intermediate $(J'M)$ and the final $(JM+1)$ level. Similarly, Fig. 4 presents the interfering channels for the creation of $\sigma_{(J'M)(JM-1)}$.

Population equations for the final $(v=2,J,M)$, the intermediate $(v=1,J',M)$, and the initial $(v=0,J'',M)$ rovibrational levels are given by

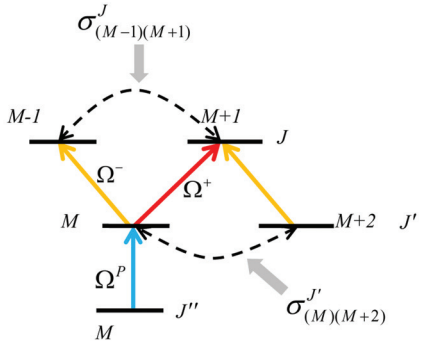

Excitation Channels Creating

$\sigma_{(J'M)(JM+1)}$

$\Omega^+ \times (\rho^{J}_{M+1} - \rho^{J'}_{M})$ ⟸ Driven by Population Difference

+

$\Omega^- \times \sigma^{J}_{(M-1)(M+1)}$ ⟸ Driven by Upper Level Zeeman Coherence

+

$\sigma^{J'}_{(M)(M+2)} \times \Omega^-$ ⟸ Driven by Intermediate Level Zeeman Coherence

+

$\Omega^{P*} \times \sigma_{(J''M)(JM+1)}$ ⟸ Driven by Two-Photon Coherence

FIG. 3. Interaction diagram showing four interfering pathways to generate the optical coherence $\sigma_{(J'M)(JM+1)}$. For details, see Ref. 18.

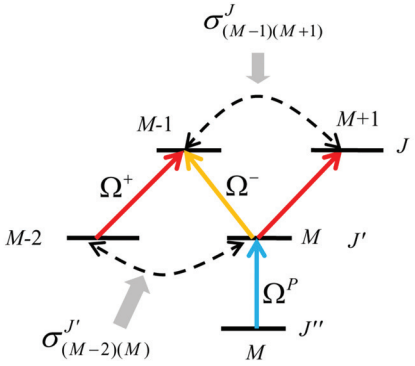

Excitation Channels Creating

$\sigma_{(J'M)(JM-1)}$

$\Omega^- \times (\rho^{J}_{M-1} - \rho^{J'}_{M})$ ⟸ Driven by Population Difference

+

$\Omega^+ \times \sigma^{J}_{(M+1)(M-1)}$ ⟸ Driven by Upper Level Zeeman Coherence

+

$\sigma^{J'}_{(M)(M-2)} \times \Omega^+$ ⟸ Driven by Intermediate Level Zeeman Coherence

+

$\Omega^{P*} \times \sigma_{(J''M)(JM-1)}$ ⟸ Driven by Two-Photon Coherence

FIG. 4. Interaction diagrams showing four interfering pathways generating the optical coherence $\sigma_{(J'M)(JM-1)}$. For details, see Ref. 18.

$$\frac{d\rho^{J}_{M}}{dt} = 2\ \mathrm{Re}\{i\Omega^{+*}_{(J'M-1)(JM)}\sigma_{(J'M-1)(JM)} + i\Omega^{-*}_{(J'M+1)(JM)}\sigma_{(J'M+1)(JM)}\}, \tag{7}$$

$$\frac{d\rho^{J'}_{M}}{dt} = 2\ \mathrm{Re}\{i\Omega^{P*}_{(J''M)(J'M)}\sigma_{(J''M)(J'M)} - i\Omega^{+*}_{(J'M)(JM+1)}\sigma_{(J'M)(JM+1)} - i\Omega^{-*}_{(J'M)(JM-1)}\sigma_{(J'M)(JM-1)}\}, \tag{8}$$

$$\frac{d\rho^{J''}_{M}}{dt} = 2\ \mathrm{Re}\{i\Omega^{P}_{(J''M)(J'M)}\sigma_{(J'M)(J''M)}\}. \tag{9}$$

Figures 3 and 4 and similar interaction diagrams are used to derive the following equations for the off-diagonal density matrix elements:

$$\frac{d}{dt}\sigma_{(J'M)(JM+1)} + \mathrm{i}\Delta_S\sigma_{(J'M)(JM+1)} = i\Omega^{+}_{(J'M)(JM+1)}(\rho^{J}_{M+1} - \rho^{J'}_{M}) + i\Omega^{-}_{(J'M)(JM-1)}\sigma^{J}_{(M-1)(M+1)} - i\Omega^{-}_{(J'M+2)(JM+1)}\sigma^{J'}_{(M)(M+2)} + i\Omega^{P*}_{(J''M)(J'M)}\sigma_{(J''M)(JM+1)}, \tag{10}$$

$$\frac{d}{dt}\sigma_{(J'M)(JM-1)} + \mathrm{i}\Delta_S\sigma_{(J'M)(JM-1)} = i\Omega^{-}_{(J'M)(JM-1)}(\rho^{J}_{M-1} - \rho^{J'}_{M}) + i\Omega^{+}_{(J'M)(JM+1)}\sigma^{J}_{(M+1)(M-1)} - i\Omega^{+}_{(J'M-2)(JM-1)}\sigma^{J'}_{(M)(M-2)} + i\Omega^{P*}_{(J''M)(J'M)}\sigma_{(J''M)(JM-1)}, \tag{11}$$

$$\frac{d}{dt}\sigma_{(J''M)(J'M)} + \mathrm{i}\Delta_P\sigma_{(J''M)(J'M)} = i\Omega^{P}_{(J''M)(J'M)}(\rho^{J'}_{M} - \rho^{J''}_{M}) - i\Omega^{+*}_{(J'M)(JM+1)}\sigma_{(J''M)(JM+1)} - i\Omega^{-*}_{(J'M)(JM-1)}\sigma_{(J''M)(JM-1)}, \tag{12}$$

$$\frac{d}{dt}\sigma^{J'}_{(M)(M+2)} + \gamma_m\sigma^{J'}_{(M)(M+2)} = i\Omega^{+}_{(J'M)(JM+1)}\sigma_{(JM+1)(J'M+2)} - i\Omega^{-*}_{(J'M+2)(JM+1)}\sigma_{(J'M)(JM+1)}, \tag{13}$$

TABLE I. Definitions of the terms found in Eqs. (7)–(16).

Symbol	Definition
ρ_M^J	Fractional population of magnetic sublevel M in the final level $(v=2,J)$.
$\rho_M^{J'}$	Fractional population of magnetic sublevel M in the intermediate level $(v=1,J')$.
$\rho_M^{J''}$	Fractional population of magnetic sublevel M in the initial level $(v=0,J'')$.
$\sigma_{(J'M)(JM+1)}(\omega_S)$	Optical coherence at frequency ω_S between levels $(v=1,J',M)$ and $(v=2,J,M+1)$.
$\sigma_{(J'M)(JM-1)}(\omega_S)$	Optical coherence at frequency ω_S between levels $(v=1,J',M)$ and $(v=2,J,M-1)$
$\sigma_{(J''M)(J'M)}(\omega_P)$	Optical coherence at frequency ω_P between levels $(v=0,J'',M)$ and $(v=1,J',M)$.
$\sigma_{(J''M)(JM+1)}(\omega_P+\omega_S)$	Two-photon coherence at frequency $(\omega_P+\omega_S)$ between levels $(v=0,J'',M)$ and $(v=2,J,M+1)$.
$\sigma_{(J''M)(JM-1)}(\omega_P+\omega_S)$	Two-photon coherence at frequency $(\omega_P+\omega_S)$ between levels $(v=0,J'',M)$ and $(v=2,J,M-1)$.
$\sigma^{J'}_{(M)(M+2)}(\omega=0)$	Zeeman coherence between the magnetic sublevels M and $M+2$ of the intermediate rovibrational level $(v=1,J')$.
$\sigma^{J}_{(M)(M+2)}(\omega=0)$	Zeeman coherence between the magnetic sublevels M and $M+2$ of the final rovibrational level $(v=2,J)$.
$\Omega^{+}_{(J'M)(JM+1)}$	Rabi frequency for σ^+ transition between levels $(J'M)$ and $(JM+1)$.
$\Omega^{-}_{(J'M)(JM-1)}$	Rabi frequency for σ^- transition between levels $(J'M)$ and $(JM-1)$
$\Omega^{P}_{(J''M)(J'M)}$	Rabi frequency for π transition between levels $(J''M)$ and $(J'M)$.
$\Delta_S=(\omega_S-\omega_{21})-i\Gamma_{12}$	Complex detuning for the $(v=1,J')\rightarrow(v=2,J)$ transition.
Γ_{12}	Dephasing rate for optical coherence $\sigma_{(J'M')(JM)}$ between the intermediate and the final level.
$\Delta_P=(\omega_P-\omega_{10})-i\Gamma_{01}$	Complex detuning for the $(v=0,J'')\rightarrow(v=1,J')$ transition.
Γ_{01}	Dephasing rate for optical coherence $\sigma_{(J''M'')(J'M')}$ between the ground and intermediate levels.
$\Delta_2=(\omega_S+\omega_P)-\omega_{20}-i\Gamma_{02}$	Complex detuning for the $(v=0,J'')\rightarrow(v=2,J)$ transition.
Γ_{02}	Dephasing rate for the optical coherence $\sigma_{(J''M'')(JM)}$ between the ground and the final rovibrational levels.
γ_m	Dephasing rate for the sublevel coherence of the intermediate and final levels which is assumed to be the same for all sublevels. This is also the dephasing rate for the molecular polarization.

$$\frac{d}{dt}\sigma^{J}_{(M)(M+2)}+\gamma_m\sigma^{J}_{(M)(M+2)}=i\Omega^{-*}_{(J'M+1)(JM)}\sigma_{(J'M+1)(JM+2)}-i\Omega^{+}_{(J'M+1)(JM+2)}\sigma_{(JM)(J'M+1)}, \tag{14}$$

$$\frac{d}{dt}\sigma_{(J''M)(JM-1)}+i\Delta_2\sigma_{(J''M)(JM-1)}=i\Omega^{P}_{(J''M)(J'M)}\sigma_{(J'M)(JM-1)}-i\Omega^{-}_{(J'M)(JM-1)}\sigma_{(J''M)(J'M)}, \tag{15}$$

$$\frac{d}{dt}\sigma_{(J''M)(JM+1)}+i\Delta_2\sigma_{(J''M)(JM+1)}=i\Omega^{P}_{(J''M)(J'M)}\sigma_{(J'M)(JM+1)}-i\Omega^{+}_{(J'M)(JM+1)}\sigma_{(J''M)(J'M)}. \tag{16}$$

Table I offers definitions of the various terms in Eqs. (7)–(16).

For IR STIRAP, we are interested in transitions for which the two-photon resonance condition is met, i.e., $(\omega_P+\omega_S)-\omega_{20}=0$, and the near or complete resonance is maintained for the intermediate transitions, i.e., $\omega_S\approx\omega_{21}$ and $\omega_P\approx\omega_{10}$. In Sec. III, we integrate Eqs. (7)–(16) numerically in the presence of the counterintuitive sequence of infrared pulses such that the pulse at frequency $\omega_S\approx\omega_{21}$ is applied before the pulse at frequency $\omega_P\approx\omega_{10}$. The population transfer and molecular alignment in the final level with $J=2$, 5, and 10 is calculated using CO in a molecular beam as the test sample.

III. POPULATION TRANSFER AND ALIGNMENT OF CO MOLECULES USING IR STIRAP

Given the collision-free ambience of a supersonic molecular beam, we ignore the dephasing of the induced coherence for an interaction time of ~1 or 2 μs. For simplicity, we also neglect the laser linewidth and assume perfect single-photon and two-photon resonance conditions. A Gaussian optical field of the form $E(t)=\exp[-(t/\tau_P)^2]$ is assumed. The pulse length τ_P is determined by the transit time through the cw laser beam, i.e., $\tau_P=w/v$, where w is the beam waist and v (~1000 m/s) is the supersonic speed of the molecule. In this study we assume a laser beam waist $w\approx1$ mm, consistent with the interaction time of ~1 μs. We have taken the vibrational dipole moment of CO for the $(v=0\rightarrow v=1)$ transition to be $\mu_{01}=0.106$ D and for the $(v=1\rightarrow v=2)$ transition to be $\mu_{12}=0.144$ D using 2004 HITRAN (High Resolution Infrared Transmission) data.[19]

For an $S(J-2)$ transition from $(J''=J-2)\rightarrow J$, the Rabi frequencies are given by

$$\Omega^{P}_{(J''M)(J'M)}=\frac{\mu_{01}E_P}{\hbar}\sqrt{\frac{(J-M-1)(J+M-1)}{(2J-1)(2J-3)}}, \tag{17a}$$

$$\Omega^{+}_{(J'M)(JM+1)}=\frac{\mu_{12}E_+}{\hbar}\sqrt{\frac{(J+M)(J+M+1)}{2(2J-1)(2J+1)}}, \tag{17b}$$

$$\Omega^{-}_{(J'M)(JM-1)}=\frac{\mu_{12}E_-}{\hbar}\sqrt{\frac{(J-M)(J-M+1)}{2(2J-1)(2J+1)}}, \tag{17c}$$

where $E_\pm=\mp E_S/\sqrt{2}$ are the amplitudes of the phase correlated circular fields $\hat{\sigma}^+$ and $\hat{\sigma}^-$ as defined in Eqs. (5a) and (5b). It is assumed that E_S and E_P both have the Gaussian temporal profile of width ~1 μs. A MATLAB program is used to integrate Eqs. (7)–(16) for an arbitrary rotational angular momentum J.

The total population of a rovibrational level (vJ) is given by

$$N_J = \sum_{M=-J}^{J} \rho_M^J. \tag{18}$$

The second-order alignment parameters $A_0^{(2)}$ and $A_{\pm 2}^{(2)}$ are used to obtain the spatial distribution for the angular momentum polarization, which is given by[12,13]

$$P(\theta,\varphi) = \frac{1}{4\pi}\Big[1 + \tfrac{5}{2}A_0^{(2)}(3\cos^2\theta - 1) + 5\sqrt{\tfrac{3}{2}}A_2^{(2)}\sin^2\theta\cos 2\varphi\Big]. \tag{19}$$

From Eq. (19) it can be seen that the parameter $A_2^{(2)}$ is responsible for breaking the cylindrical symmetry for the spatial distribution of the angular momentum $\boldsymbol{J}$. In the following, we show that the alignment parameter $A_{\pm 2}^{(2)}$ becomes most important for the molecular polarization in high-J states. The results of the numerical calculations are presented in Figs. 5–7 for CO ($v=2$, $J=2$, 5, and 10).

The simplest case of an S(0) transition corresponds to $J=2$ with four interacting quantum levels. Figure 5(a) shows complete population transfer to the level ($v=2$, $J=2$) using a delayed pulse sequence in the counterintuitive sense, where the resonant optical field $E_S(\omega_S)$ for the ($v=1$, $J'=1$) $\rightarrow$($v=2$, $J=2$) transition is applied prior to the optical field $E_P(\omega_P)$ coupling the ($v=0$, $J''=0$)$\rightarrow$($v=1$, $J'=1$) transition. For the pulse duration $\tau_P=1$ μs, the optimum delay between the pulses is 1 μs.[8] A peak vibrational Rabi frequency $\Omega_S=\Omega_P=\mu_{01}E_P/\hbar=1.2$ MHz is used corresponding to a pulse area $\Omega\tau_P\approx 7.5$ rad at a laser power of $\sim$30 mW/mm^2. The pulse area fulfills the adiabatic following condition $\Omega\tau \gg 1$ for the adiabatic eigenstate of the RWA Hamiltonian representing a four-level molecular system. It should be noted that the orientation or M-dependent Rabi frequencies and the pulse areas for π and σ transitions are scaled by the appropriate orientational factors, the Clebsch–Gordan coefficients, which are included in the calculation. Figure 6(a) shows the final Zeeman population distribution in the final rovibrational level $v=2$, $J=2$ at the end of the pulse sequence. Figure 7(a) shows the three-dimensional polar plot of the angular momentum polarization obtained with two perpendicularly polarized laser beams propagating along the $\hat{y}$-axis. The quantization $\hat{z}$-axis is oriented along the polarization direction of the optical field tuned to the ($v=0$, $J''=0\rightarrow v=1$, $J'=1$) π transition. The alignment parameters for the S(0) transition are found to be $A_0^{(2)}\cong -0.5$ and $A_{\pm 2}^{(2)}\cong -0.6$, which is in agreement with our previous study on a four-level molecular system.[8] This validates the generalized density matrix treatment and the numerical analysis for the arbitrary values of J.

The STIRAP dynamics for an S(3) transition involves 27 different quantum levels. The ground and the intermediate levels are connected using the π transitions, while the intermediate and final levels are coupled by the σ transitions. Figure 5(b) shows that approximately 94% population transfer can be achieved using a vibrational Rabi frequency of $\Omega=1.8$ MHz at a laser power of $\sim$67 mW/mm^2. Increasing the Rabi frequency or the laser power does not increase the population transfer. As it is seen also for $J=10$, the maximum population transfer in a STIRAP process with highly degenerate rotational states is influenced by the quantum interference of excitation channels. In an N-type interaction, the Zeeman coherence couples the excitation channels affecting the optical transition between the intermediate and final levels. The quantum interference in an N-type interaction is well studied in relation to the electromagnetically induced transparency and absorption.[20–22] Although the Zeeman coherence limits the population transfer in a highly degenerate STIRAP process, it becomes the key player in inducing sig-

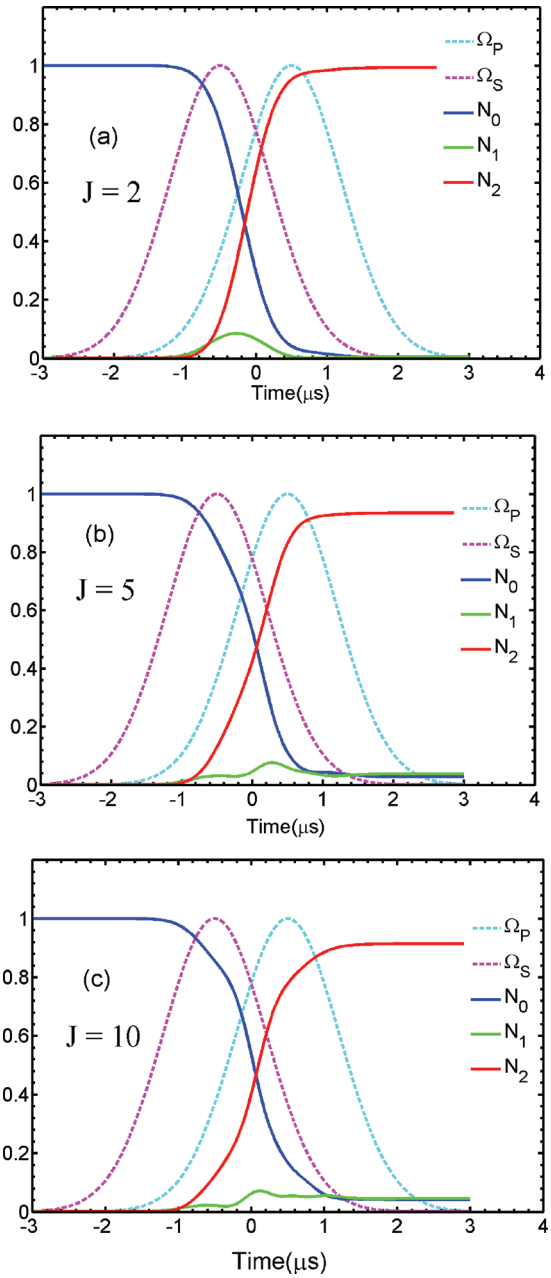

FIG. 5. Nearly complete population transfer to the ($v=2$,J) level using S($J-2$) IR STIRAP with the counterintuitive sequence of Gaussian pulses of duration 1 μs and interpulse delay of 1 μs for (a) $J=2$ with Rabi frequency $\Omega=1.2$ MHz, laser intensity 30 mW/mm^2, and population transfer of 100%; (b) $J=5$ with Rabi frequency $\Omega=1.8$ MHz, laser intensity 67 mW/mm^2, and population transfer of 94%; and (c) $J=10$ with Rabi frequency $\Omega=2.2$ MHz, laser intensity 100 mW/mm^2, and population transfer of 92%.

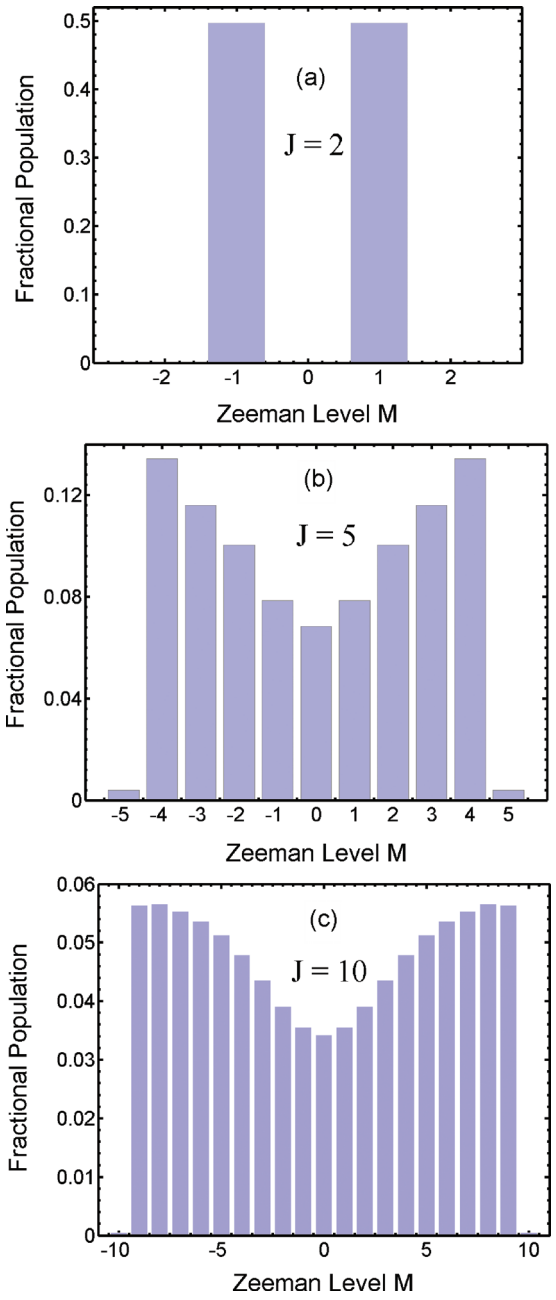

FIG. 6. Zeeman population distribution in the final level $(v=2,J)$ using S$(J-2)$ IR STIRAP at the end of excitation with the counterintuitive sequence of Gaussian pulses of duration 1 μs and interpulse delay of 1 μs: (a) $J=2$; (b) $J=5$; and (c) $J=10$. Rabi frequencies and laser power for each S$(J-2)$ transition are the same as in Fig. 5.

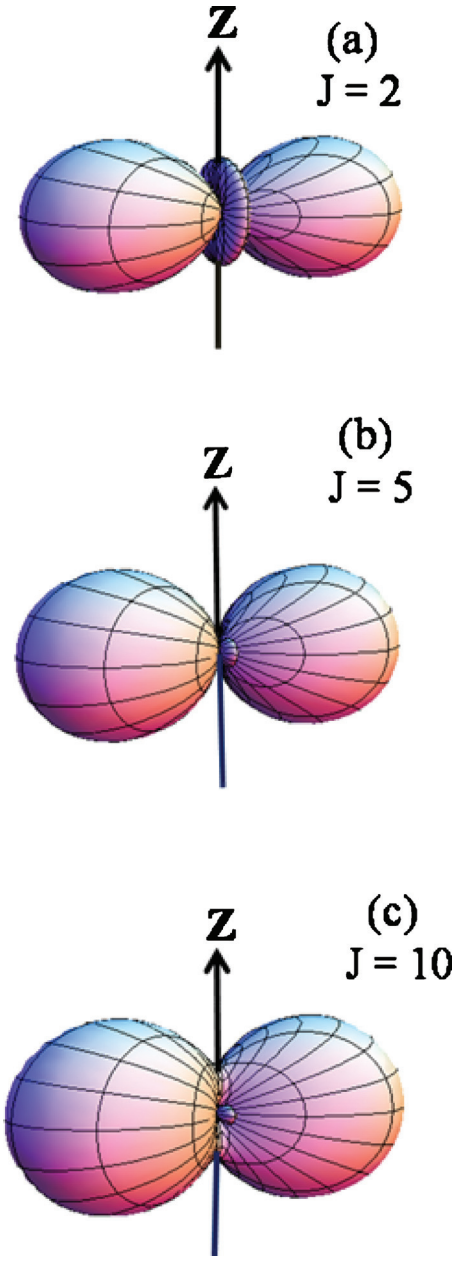

FIG. 7. Three-dimensional polar plot of the angular momentum polarization in the final $(v=2,J)$ level using S$(J-2)$ IR STIRAP with the counterintuitive sequence of Gaussian pulses for (a) $J=2$ with alignment parameters $A^{(2)}_0=-0.5$ and $A^{(2)}_{\pm 2}=-0.61$; (b) $J=5$ with alignment parameters $A^{(2)}_0=-0.19$ and $A^{(2)}_{\pm 2}=-0.35$; and (c) $J=10$ with alignment parameters $A^{(2)}_0=-0.07$ and $A^{(2)}_{\pm 2}=-0.27$. The pulse duration, delay, and laser power are identical to those of Figs. 5 and 6.

nificant polarization for the vibrationally excited molecular ensemble. Figure 6(b) shows the Zeeman population distribution and Fig. 7(b) shows the three-dimensional polar plot of the angular momentum polarization. The calculated alignment parameters are $A^{(2)}_0=-0.19$ and $A^{(2)}_{\pm 2}=-0.35$. The ratio $A^{(2)}_2/A^{(2)}_0$ increases as we involve more coupled levels with higher rotational quantum number J, which implies a stronger azimuthal ϕ confinement.

Lastly, we consider the angular momentum polarization in the $v=2$, $J=10$ rovibrational level using an S(8) IR STIRAP process involving 57 quantum levels. Figure 5(c) shows that under suitable condition using a vibrational Rabi frequency $\Omega=2.2$ MHz and a cw infrared power of 100 mW/mm^2 per laser beam, a maximum of $\sim$92% population is transferred to the $(v=2,\ J=10)$ level. Increasing the laser power does not improve the population transfer as the limit arises from the interference of quantum pathways, which depends mostly on relative phases rather than amplitudes. Figure 6(c) shows the Zeeman population distribution in the final level. It is very interesting to note that the Zeeman population is almost uniform resulting in an alignment parameter $A^{(2)}_0=-0.07$. However, there is substantial spatial confinement of $\boldsymbol{J}$ caused by the Zeeman coherence expressed

by the alignment parameter $A^{(2)}_{\pm 2}=-0.27$. Figure 7(c) shows the three-dimensional polar plot of the angular momentum distribution, i.e., the $\boldsymbol{J}$-polarization.

The role of the Zeeman coherence becomes even more spectacular when we consider the IR STIRAP process for $J=20$. The calculation yields the alignment parameters $A^{(2)}_0=-0.003$ and $A^{(2)}_{\pm 2}=-0.24$, suggesting stronger squeezing of the $\boldsymbol{J}$-polarization in the $\hat{x}$-direction. For $J=20$, as much as 91% of the population can be transferred to the $(v=2,\ J=20)$ rovibrational level using a laser power of $\sim 200\ \mathrm{mW/mm^2}$.

In the STIRAP literature,[9–11] it is often claimed that 100% population transfer occurs. This statement is true in the absence of coupling between different M-sublevels, for example, for two parallel π-polarized transitions (Fig. 1). As shown above, this statement is not completely correct in general. For IR STIRAP with π-polarized and $\sigma^{\pm}$-polarized photons, the N-type interactions between the M-sublevels prevent complete population transfer, although the population transfer remains large.

IV. DISCUSSION

In this work, we have shown that Zeeman coherence (M-sublevel entanglement) creates significant molecular polarization. Using the infrared STIRAP with $\hat{z}$- and $\hat{x}$-polarized light, a highly correlated superposition of magnetic sublevels is created for an ensemble of vibrationally excited molecules in the rovibrational eigenstate $(v=2,J)$. For the molecular ensemble, the angular momentum polarization is determined by the relative phase rather than by the population distribution of the M-sublevels. For the phase correlated ensemble, the angular momentum polarization can be considered as a purely quantum mechanical effect.

IR STIRAP simultaneously achieves

(1) Nearly complete population transfer to a single rovibrational eigenstate $(v=2,J)$,
(2) M-state entanglement of the vibrationally excited molecules, and
(3) Angular momentum polarization arising from the entanglement.

To describe the coherence and interference in IR STIRAP interaction for a molecular ensemble with an arbitrary rotational quantum number J, we have developed a comprehensive density matrix treatment. We have numerically studied the IR STIRAP dynamics and the angular momentum polarization by considering the excitation of CO molecules in a supersonic molecular beam with a sequence of delayed infrared pulses applied in a counterintuitive manner. We find that the population transfer in this IR STIRAP process for a highly degenerate quantum system is influenced by the M-sublevel (Zeeman) coherence. For $J=10$, a maximum population transfer of 92% is obtained at a laser power level of $100\ \mathrm{mW/mm^2}$. Because the limit on the population transfer arises from the quantum interference of excitation channels, it cannot be removed or improved by increasing the optical power. In the presence of almost uniform population distribution, the angular momentum distribution is nevertheless polarized and the extent of polarization arises essentially from the phase correlation of the M-sublevels.

We believe that the IR STIRAP offers a general and a practical way for creating polarized molecular targets. It should also be appreciated that IR STIRAP can be used to climb higher in the vibrational ladder to create entanglement and alignment for a molecular ensemble in highly excited vibrations levels, such as $v=4$ level or greater, although this requires several coherent infrared beams to operate together.

ACKNOWLEDGMENTS

This work was supported by the National Science Foundation and the Army Research Office.

[1] R. E. Drullinger and R. N. Zare, J. Chem. Phys. **51**, 5532 (1969); **59**, 4225 (1973).
[2] R. N. Zare, Ber. Bunsenges. Phys. Chem. **86**, 422 (1982).
[3] R. Altkorn and R. N. Zare, Annu. Rev. Phys. Chem. **35**, 265 (1984).
[4] Ke-Li Han, Phys. Rev. A **56**, 4992 (1997).
[5] N. C. M. Bartlett, D. J. Miller, R. N. Zare, D. Sofikitis, T. P. Rakitzis, and A. J. Alexander, J. Chem. Phys. **129**, 084312 (2008).
[6] F. Legare, S. Chelkowski, and A. D. Bandrauk, Chem. Phys. Lett. **329**, 469 (2000).
[7] C. H. Greene and R. N. Zare, Annu. Rev. Phys. Chem. **33**, 119 (1982).
[8] N. Mukherjee and R. N. Zare, J. Chem. Phys. **132**, 154302 (2010).
[9] N. V. Vitanov, M. Fleischhauer, B. W. Shore, and K. Bergmann, Adv. At., Mol., Opt. Phys. **46**, 55 (2001).
[10] K. Bergmann, H. Theuer, and B. W. Shore, Rev. Mod. Phys. **70**, 1003 (1998) (and references therein).
[11] U. Gaubatz, P. Rudeck, S. Schiemann, and K. Bergmann, J. Chem. Phys. **92**, 5363 (1990).
[12] C. Liedenbaum, S. Stolte, and J. Reuss, Phys. Rep. **178**, 1 (1989).
[13] V. Milner and Y. Prior, Phys. Rev. A **59**, R1738 (1999).
[14] V. Milner, B. M. Chernobrod, and Y. Prior, Phys. Rev. A **60**, 1293 (1999).
[15] A. J. Orr-Ewing and R. N. Zare, Annu. Rev. Phys. Chem. **45**, 315 (1994).
[16] R. N. Zare, *Angular Momentum: Understanding Spatial Aspects in Chemistry and Physics* (Wiley/Interscience, New York/New York, 1988).
[17] F. Vewinger, M. Heinz, B. W. Shore, and K. Bergmann, Phys. Rev. A **75**, 043406 (2007).
[18] N. Mukherjee, J. Opt. Soc. Am. B **23**, 1635 (2006).
[19] L. S. Rothman, D. Jacquemart, A. Barbe, D. C. Benner, M. Birk, L. R. Brown, M. R. Carleer, C. Chackerian, Jr., K. Chance, L. H. Coudert, V. Dana, V. M. Devi, J.-M. Flaud, R. R. Gamache, A. Goldman, J.-M. Hartmann, K. W. Jucks, A. G. Maki, J.-Y. Mandin, S. T. Massie, J. Orphal, A. Perrin, C. P. Rinsland, M. A. H. Smith, J. Tennyson, R. N. Tolchenov, R. A. Toth, J. Vander Auwera, P. Varanasi, and G. Wagner, J. Quant. Spectrosc. Radiat. Transf. **96**, 139 (2005).
[20] S. E. Harris, Phys. Rev. Lett. **70**, 552 (1993).
[21] C. Y. Ye, A. S. Zibrov, Y. V. Rostovtsev, and M. O. Scully, J. Mod. Opt. **50**, 2605 (2003).
[22] A. V. Taichenachev, A. M. Tumaikin, and V. I. Yudin, Phys. Rev. A **61**, 011802(R) (1999).